Appendix C

Pd(11N) Vicinal Surfaces

C.1 Clean Pd(11N) Vicinal Surfaces

Similar to the low-index surfaces we have to test the important computational parameters to ensure the convergence of the targeted surface properties. For the surface energy γ we again focus on energy cutoff and **k**-point sampling. For these tests we use 5, 7 and 9 layer slabs for Pd(113), Pd(115) and Pd(117), respectively, which corresponds each time to the least number of layers possible, while maintaining a bulk-like coordination for the center layer in the slab. The vacuum thickness is about 20 Å, 28 Å, and 23 Å in Pd(113), Pd(115), and Pd(117), respectively. Figures C.1, C.2 and C.3 show the convergence of γ [1] with energy cutoff and number of k-points for the Pd(113), Pd(115) and Pd(117) surface, respectively. In all these cases, the surface energy is converged to within ± 0.5meV/Å^2 for $E_{\rm max}^{\rm wf} \geq$20 Ry. A similar convergence is reached for k-meshes exceeding k-meshes of $(6 \times 10 \times 1)$ for Pd(113) [2], $(2 \times 9 \times 1)$ for Pd(115), and $(2 \times 7 \times 1)$ for Pd(117), which corresponds to 32, 14 and 8 irreducible **k**-points, respectively.

For the calculation of γ, one needs not only the total energy of the slab $E_{\rm slab}^{\rm total}$, but also the total energy of a bulk atom $E_{\rm bulk}^{\rm total}$. In Fig C.1, C.2 and C.3 we used for this simply the result of a normal fcc bulk unit cell calculation. That this is not an optimum choice becomes apparent, when testing the slab thickness below. With increasing number of slab layers (while always keeping the vacuum thickness above 11 Å) the surface energy becomes larger and larger (upper panel in Fig. C.4), as discussed in *ref.* [143]. The reason lies in the slightly different sampling of the Brillouin zones in the bulk and in the surface calculation: The respective Brillouin zones are

[1] For simplicity, $E_{\rm bulk}^{\rm total}$ of fcc Pd bulk is used from a calculation with a regular fcc bulk unit cell. As described below it is more appropriate to use $E_{\rm bulk}^{\rm total}$ from a bulk calculation with a supercell geometry equivalent to the slab orientation to obtain compatible k-meshes. However, this does not affect the basis set convergence tests for one fixed slab width we are interested in here.

[2] In Fig. C.1 the k-meshes are tested in two different ways: One is using non-comparable k-meshes for the cubic fcc bulk Pd calculation, the other one is using equivalent k-meshes for the slab bulk calculation. (see discussion below)

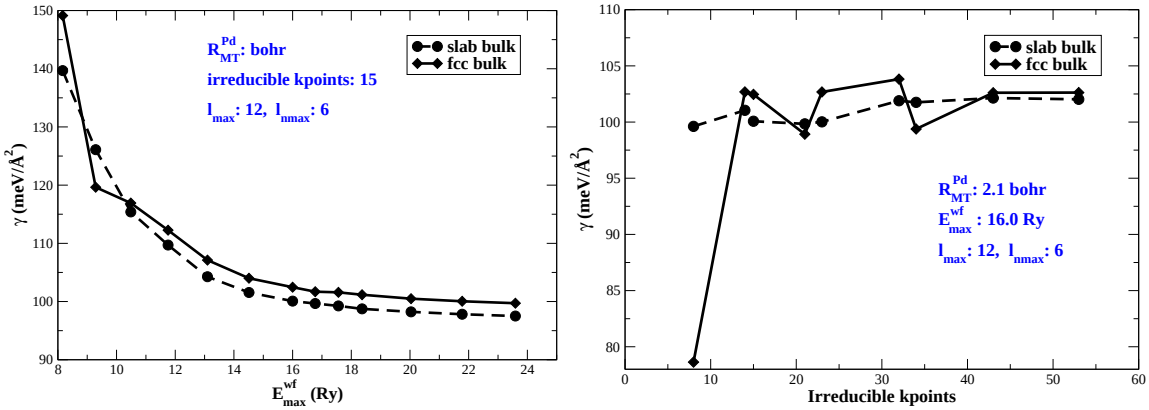

Figure C.1: Energy cutoff ($E^{\rm wf}_{\rm max}$) and irreducible k-point convergence tests for Pd(113). For a convergence within ± 0.5meV/Å^2, the optimal energy cutoff is $E^{\rm wf}_{\rm max}$=20 Ry, and the optimal irreducible k-point number is (k-mesh: $6\times10\times1$), corresponding to 32 irreducible **k**-points. Red curve and black curve are the surface energies from fcc bulk and slab bulk calculation, respectively. (see footnote 2)

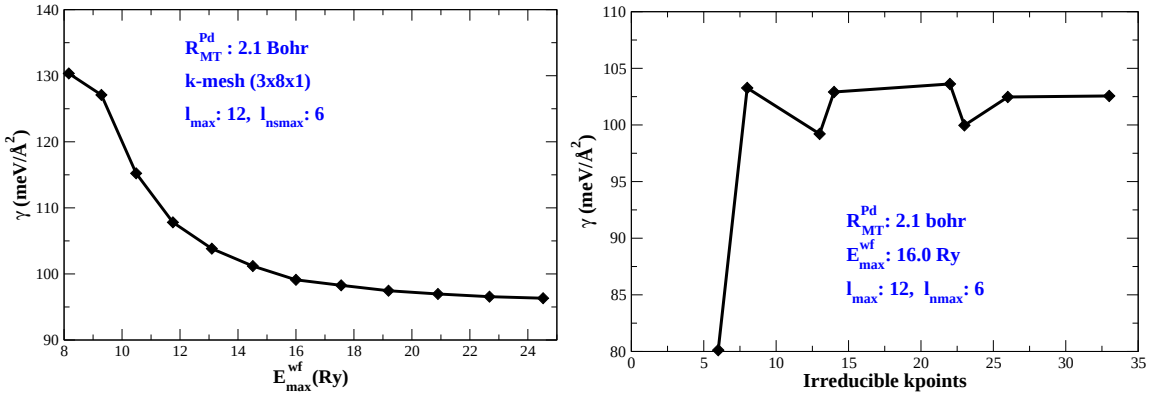

Figure C.2: Energy cutoff ($E^{\rm wf}_{\rm max}$) and irreducible k-point convergence tests for Pd(115). For a convergence within ± 0.5meV/Å^2, the optimal energy cutoff is $E^{\rm wf}_{\rm max}$=20 Ry, and the optimal irreducible k-point number is 14 (k-mesh: $3\times9\times1$), corresponding to 14 irreducible **k**-points.

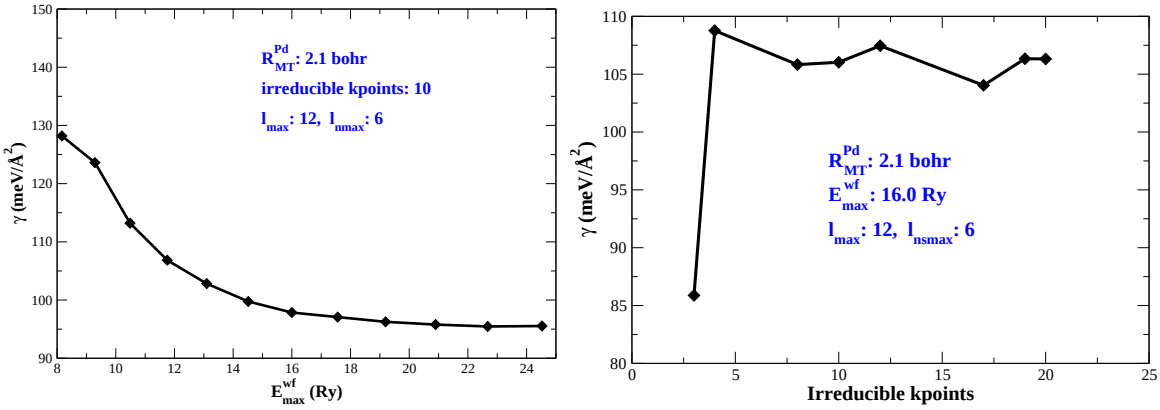

Figure C.3: Energy cutoff ($E^{\rm wf}_{\rm max}$) and irreducible k-point tests for Pd(117). For a convergence within ± 0.5meV/Å^2, the optimal energy cutoff is $E^{\rm wf}_{\rm max}$=20 Ry, and the optimal irreducible k-point number is 8 (k-mesh: $2\times7\times1$), corresponding to 8 irreducible **k**-points.

oriented differently and the Monkhorst-pack grids sample different points. Therefore the contribution of bulk-like atoms in the middle of the slab does not cancel, as they are described slightly differently by the two k-meshes. Consequently the surface energy diverges. This problem can be resolved by using for $E_{\text{bulk}}^{\text{total}}$ the total energy of an atom in a *slab bulk*, *i.e.* building a bulk Pd structure by completely filling a vicinal supercell layer by layer. The smallest number of layers required in the supercell is determined by the Miller indices of the vicinal surface, $1^2 + 1^2 + n_{\text{row}}^2$. Then the k-meshes of the two structures, slab bulk and surface slab, are equivalent, *e.g.* $(6 \times 10 \times 2)$ and $(6 \times 10 \times 1)$ in Pd(113), which minimizes errors from the k-point sampling. The surface energy obtained with this procedure is converged to within 1 meV/Å^2 already for the 5 layer slab (lower panel in Fig. C.4). In the same way, we can get similarly converged surface energies for Pd(115) (upper panel in Fig. C.5) and Pd(117) (lower panel in Fig. C.5). Equivalent k-meshes for the two structures, slab and bulk, in the surface energy equation Eq. 4.8 are therefore very important to generate converged curves. Analyzing the relaxed slabs in more detail, we find no further geometry relaxation after 9 layers, 17 layers and 19 layers for Pd(113), Pd(115) and Pd(117), respectively. Similarly, the k-meshes for the three vicinal surfaces must also be as commensurate as possible, in order to allow a meaningful comparison of the surface energetics of the three surfaces. If we take the k-mesh of Pd(113), $(6 \times 10 \times 1)$, as the standard, the task is to find the corresponding k-meshes on Pd(115) and Pd(117) using the relation of the surface unit cells. As apparent from Fig. 4.3 the angle γ is similar in the three surface unit cells, and the b distance of the three Pd(11N) surfaces is equal. The **k**-point sampling in this direction should therefore be equal, namely 10. Along the other direction, a, the proportion of their distances is about 9:14:19, therefore the **k**-point along this direction is 4 and 3 for Pd(115) and Pd(117), respectively. The equivalent k-meshes of Pd(113), Pd(115) and Pd(117) surfaces are therefore $(6 \times 10 \times 1)$, $(4 \times 10 \times 1)$ and $(3 \times 10 \times 1)$, respectively. Similar to the vacuum thickness test carried out for Pd(111) and Pd(100), we increased and decreased the vacuum thickness in the vicinal supercells. The resulting surface energies are summarized in Table C.1, from which it becomes clear that the effect of vacuum thickness beyond 10 Å is virtually zero (< 1 meV/Å^2). Therefore the vacuum thickness used already before in the basis set tests for the clean vicinal Pd(11N) surfaces is large enough to avoid the interaction between two consecutive slabs

All basis sets used in the Pd(11N) vicinal surface calculations and the corresponding surface energies are summarized in Table C.2. The final surface energies for the three vicinal surfaces are 100.3 meV/Å^2, 99.4 meV/Å^2, and 99.1 meV/Å^2, respectively. They are smaller than the surface energies of the corresponding bulk-truncated vicinal surfaces (Table C.2). Obviously the surface relaxation stabilizes the surfaces. Pd(113) has the highest surface energy among all the surfaces, which is significantly larger than the one of the close-packed Pd(111) surface. However, for increasing (100) terraces width, the surface energy of Pd(11N) becomes smaller, and we observe the trend, $\gamma_{113} > \gamma_{115} \approx \gamma_{117}$.

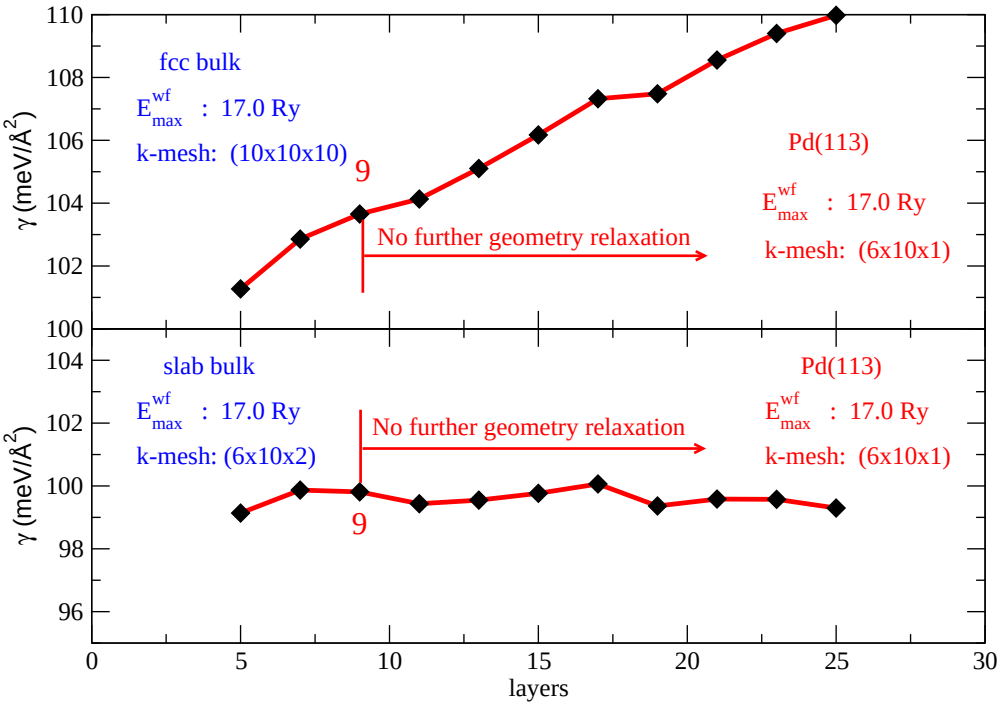

Figure C.4: Surface energy convergence with number of slab layers for the Pd(113) vicinal surface. Upper panel: Surface energy using E_{bulk} from a bulk fcc Pd unit cell calculation. Lower panel: Surface energy using E_{bulk} from a slab bulk calculation.

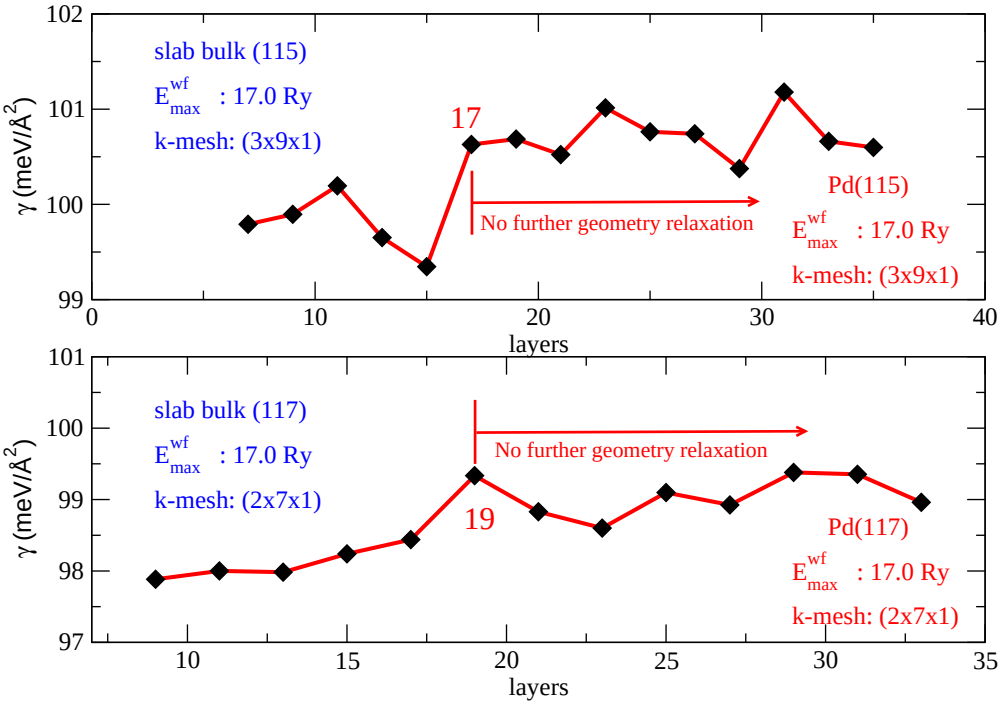

Figure C.5: Surface energy vs. slab layers for Pd(115) (upper panel) and Pd(117) (lower panel), and using $E_{\text{bulk}}^{\text{total}}$ from a slab bulk calculation.

Table C.1: Surface energies of the Pd(11N) (N=3, 5, 7) vicinal surfaces for different vacuum thicknesses, and using $E_{\max}^{\mathrm{wf}}$=17 Ry and a $(6 \times 10 \times 1)$, $(3 \times 9 \times 1)$ and $(2 \times 7 \times 1)$ for Pd(113), Pd(115) and Pd(117), respectively.

	Pd(113)			Pd(115)			Pd(117)		
Vacuum (Å)	15	30	46	11	22	32	12	24	35
γ (meV/Å^2)	99.6	99.8	99.7	100.4	100.6	100.6	99.2	99.3	99.3

Table C.2: Computed surface energies of different low-index and vicinal surfaces using optimum basis sets. (The k-meshes of Pd(11N) are equivalent).

	Pd(111)	Pd(113)	Pd(115)	Pd(117)	Pd(100)
$E_{\max}^{\mathrm{wf}}$ (Ry)	20	20	20	20	20
k-meshes	$(9 \times 9 \times 1)$	$(6 \times 10 \times 1)$	$(4 \times 10 \times 1)$	$(3 \times 10 \times 1)$	$(9 \times 9 \times 1)$
layers	7	9	17	19	7
vacuum (Å)	23	30	22	24	20
$\gamma_{\mathrm{unrelax}}$ (meV/Å^2)	87.9	100.3	99.4	99.1	96.4
γ_{relax} (meV/Å^2)	87.9	98.3	97.3	97.4	96.3

C.2 Oxygen at Pd(11N) Vicinal Surfaces

With respect to oxygen adsorption at the vicinal surfaces, we focus our convergence tests on two representative adsorption sites, namely the Thu and Sh2 sites. We test the convergence with the energy cutoff by computing the binding energy in a (1×1) cell.

The k-meshes are the same as the optimal values for the clean vicinal surfaces, $(6 \times 10 \times 1)$, $(3 \times 9 \times 1)$ and $(2 \times 7 \times 1)$ for oxygen adsorption on Pd(113), Pd(115) and Pd(117), respectively. The slab thicknesses are 13, 17 and 23 layers, and the corresponding vacuum thicknesses are 25 Å, 20 Å and 20 Å for Pd(113), Pd(115) and Pd(117), respectively. From Fig. C.6, it becomes clear that the absolute binding energies of the oxygen atoms at each site show the same convergence trend. Unfortunately, both of them converge quite slowly, and the $E_{\max}^{\mathrm{wf}}$ curves show a convergence to within 50 meV only above 26 Ry. In contrast, the relative binding energy difference between the two sites (insert panel in Fig. C.6) is already converged to within 5 meV above 20 Ry. In our work we focus on the most favorable site for the oxygen atoms on the Pd(11N) surfaces. This trend only requires converged relative binding energies and we choose 20 Ry as the optimal energy cutoff for the oxygen adsorption at Pd(113), which yields accurate relative binding energy differences at an affordable computational time. In the same spirit, we calculate the binding energy of oxygen

at the Sh2 site on Pd(115) and Pd(117) (Fig. C.7), and compare the results with the binding energies at the same site on Pd(113) (insert panel in Fig. C.7). From the figure we see that the absolute binding energy of oxygen on Pd(115) and Pd(117) shows a similar trend as oxygen on Pd(113): slow convergence of the absolute values, while the relative differences reach a convergence to within 5 meV at $E_{\max}^{\mathrm{wf}}$=20.0 Ry. We conclude that for our study 20 Ry is an optimal energy cutoff for the oxygen adsorption on all three Pd(11N) surfaces.

Next, the required number of slab layers are tested using the other optimal parameters (energy cutoff and k-mesh) of the clean vicinal surfaces. The thickness of the chosen supercell is 40.47 Å, 33.43 Å and 33.16 Å for the oxygen adsorption on Pd(113), Pd(115) and Pd(117), respectively. This size is kept fixed despite the increasing number of slab layers. Although the vacuum thickness becomes thus smaller and smaller, the least vacuum thickness is 12 Å, 11 Å and 16 Å for oxygen on Pd(113), Pd(115) and Pd(117), respectively, which is still large enough (see vacuum test below). For the oxygen adsorption on Pd(113) surface we also increased the k-mesh from ($6 \times 10 \times 1$) to ($8 \times 14 \times 1$) to check if the old k-mesh is good enough for the adsorption system. In Fig. C.8 the binding energy curves at the two adsorption sites (Sh2 and Thu) are nicely converged with increasing number of slab layers. The two curves show the same convergence trend, and the binding energy is converged to within 10 meV already for 13 layers for the two adsorption sites. Moreover, the high k-mesh ($8 \times 14 \times 1$) generates the same trend as the lower k-mesh ($6 \times 10 \times 1$) does, and the binding energies from the two k-meshes are nearly the same, when the number of layers is more than the optimal layers. We therefore identify the ($6 \times 10 \times 1$) mesh as good enough to study the oxygen adsorption at Pd(113). In the same way, we increase the ($3 \times 9 \times 1$) and ($2 \times 7 \times 1$) meshes to ($4 \times 12 \times 1$) and ($3 \times 10 \times 1$) to check the **k**-points sampling for oxygen at Pd(115) and Pd(117), respectively (Fig. C.9). The binding energies of the two kinds of k-meshes are similar, and the difference is less than 20 meV throughout. Therefore, ($3 \times 9 \times 1$) and ($2 \times 7 \times 1$) k-meshes are enough to study the oxygen adsorption at Pd(115) and Pd(117), respectively. Fig. C.9 (oxygen adsorption on Pd(115) and Pd(117)) shows furthermore the same trend as oxygen adsorption on Pd(113): The two binding energy curves at the two adsorption sites rapidly converge with increasing number of slab layers, and the binding energy is converged to within 10 meV for the same optimal layer number. Therewith, 17 layers and 23 layers are the optimal number of slab layers for the oxygen adsorption on Pd(115) and Pd(117), respectively. Finally, we test the vacuum thicknesses of the three kinds of oxygen adsorption systems by increasing and decreasing the vacuum thickness. All corresponding binding energies are tabulated in Table C.3, from which it is clear that the effect of vacuum thickness is negligible (<10 meV) beyond 12 Å, 10 Å and 10 Å for the oxygen adsorption at the Sh2 site on Pd(113), Pd(115) and Pd(117), respectively. As mentioned in the tests of clean Pd(11N) vicinal surfaces, in order to compare quantities, like binding energies, in the family of Pd(11N) vicinal surfaces the k-meshes of the three adsorption systems should be comparable. Therefore, ($6 \times 10 \times 1$), ($4 \times 10 \times 1$) and ($3 \times 10 \times 1$) are used for the oxygen adsorption on Pd(113), Pd(115) and Pd(117),

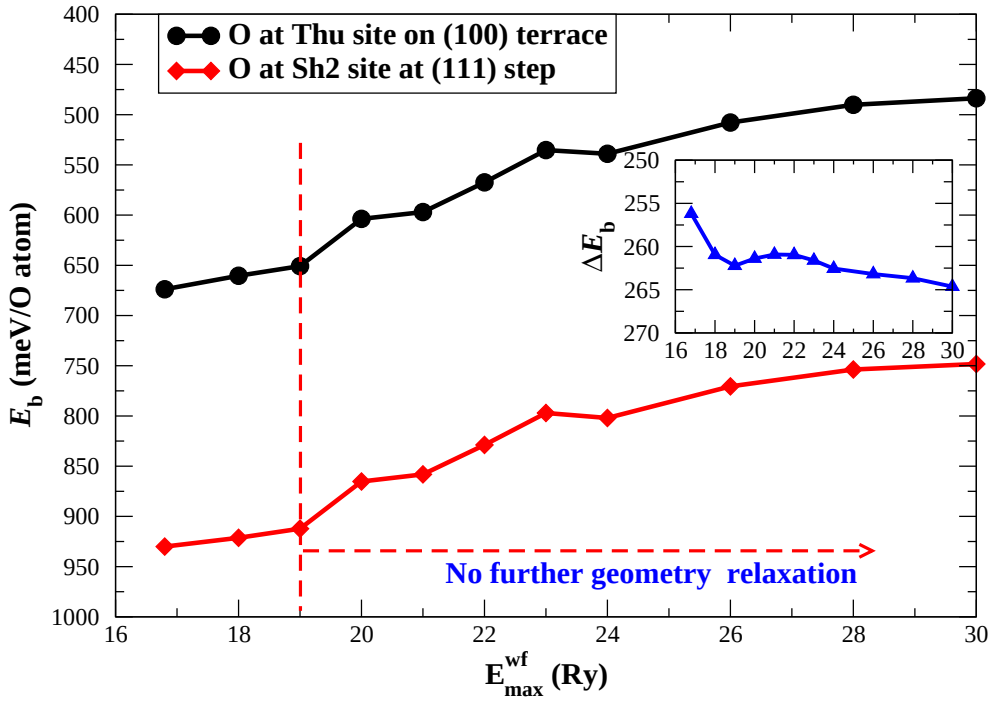

Figure C.6: Absolute binding energies of oxygen adsorbed at the Sh2 and Thu sites at Pd(113) with different energy cutoff values. The insert panel shows the relative binding energy of the two sites.

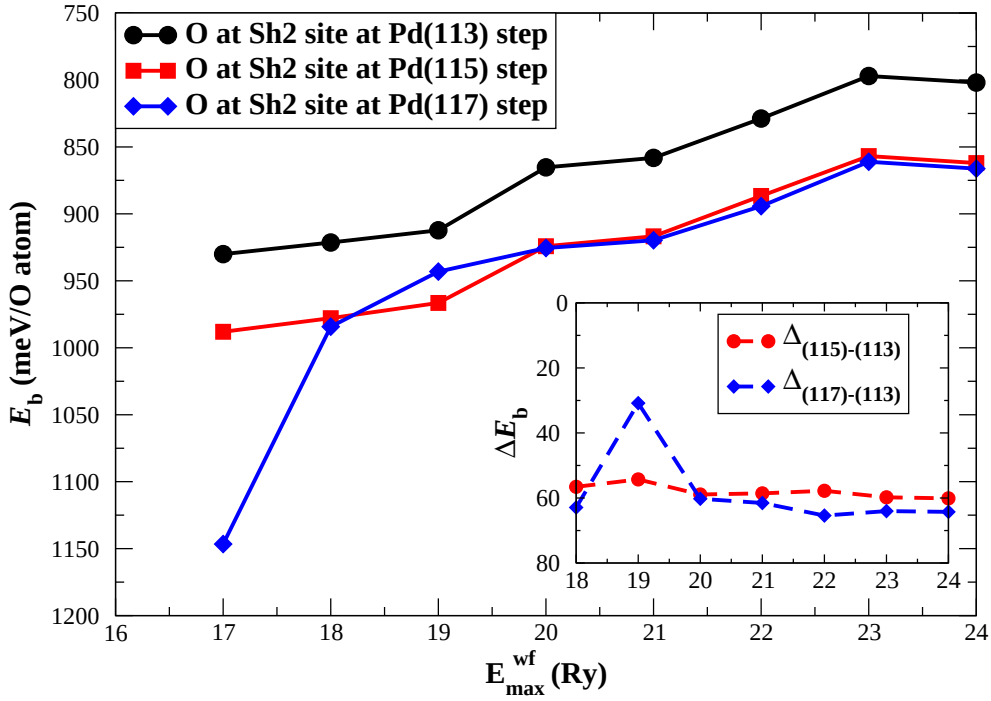

Figure C.7: Binding energy vs. energy cutoff for oxygen adsorbed at the Sh2 site at Pd(113), Pd(115) and Pd(117). The insert shows the relative binding energy with respect to oxygen at the Sh2 site at Pd(113).

Table C.3: Binding energies for various vacuum thicknesses in supercells for the oxygen adsorption at the Sh2 site.

	1O-Pd(113)(1×1)			1O-Pd(115)(1×1)			1O-Pd(117)(1×1)		
Vacuum (Å)	37	25	12	30	20	10	30	20	10
E_b (meV)	875	875	874	923	924	929	927	926	933

Table C.4: Optimal basis set parameters of oxygen adsorption on Pd(11N) surfaces.

	energy cutoff (Ry)	k-mesh	vacuum thickness (Å)	slab layers
1O-Pd(113)(1×1)	20	$6 \times 10 \times 1$	25	13
1O-Pd(115)(1×1)	20	$4 \times 10 \times 1$	20	17
1O-Pd(117)(1×1)	20	$3 \times 10 \times 1$	20	23

respectively. At last, we summarize the optimal basis set parameters in Table C.4.

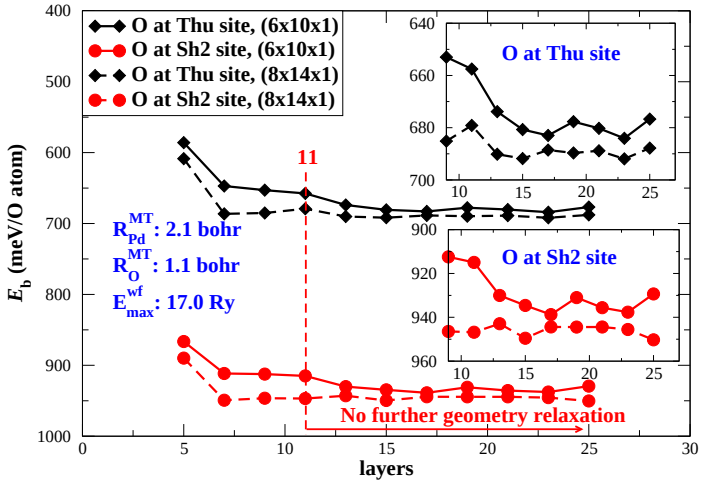

Figure C.8: Convergence of the binding energy with increasing number of slab layers for oxygen adsorption at the two adsorption sites (Sh2 and Thu) on Pd(113) surface. Solid and dashed lines indicate two kinds of k-meshes, $(6 \times 10 \times 1)$ and $(8 \times 14 \times 1)$, respectively.

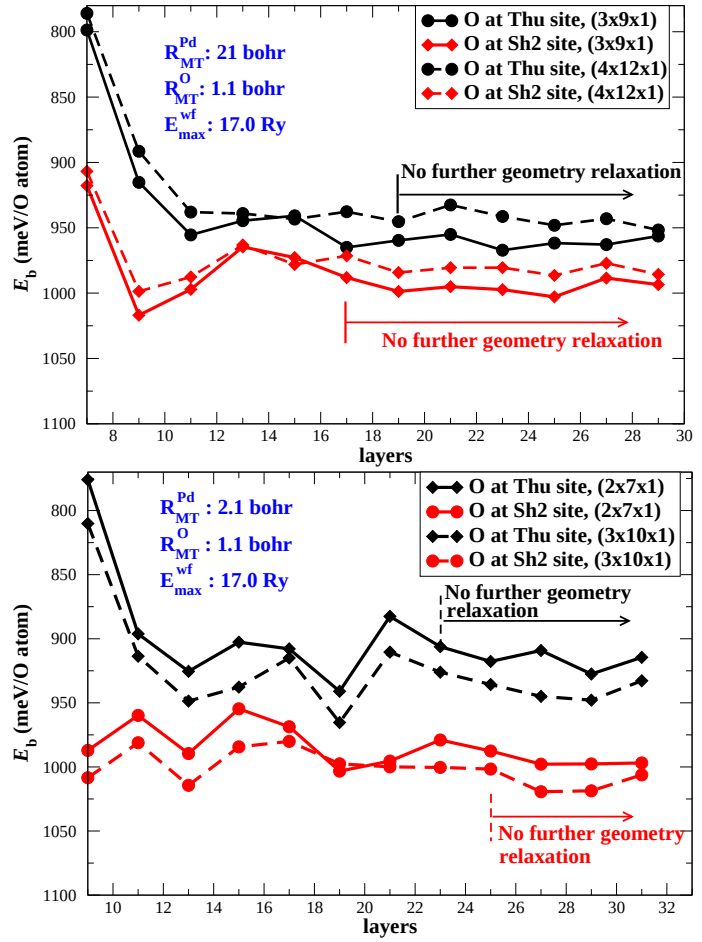

Figure C.9: Convergence of the binding energy with the number of slab layers for oxygen adsorption at Sh2 and Thu sites on Pd(115) (upper panel) and on Pd(117) (lower panel).